An enhanced forced vibration rig for wind tunnel testing of bridge deck section models in arbitrary motion

Bartosz Siedziako, Ole Øiseth, Anders Rønnquist

Department of Structural Engineering, Norwegian University of Science and Technology, Trondheim, Richard Birkelands vei 1A, 7491 Trondheim Norway

Published in: Journal of Wind Engineering and Industrial Aerodynamics
DOI: 10.1016/j.jweia.2017.02.011

Abstract
This paper presents a new experimental setup for the aerodynamic section model testing of bridge decks. The rig is designed to move a section model in arbitrary motion in a wind tunnel to imitate the motions of such scaled real bridge motion, step motion or random motion histories to be close to white noise. The proposed setup enables the forces acting on the section model to be measured directly while considering motions that resemble actual bridge motion and still fully utilizing the benefits of the forced vibration testing technique. The excellent performance of the system and testing procedure is proved by performing state-of-the-art forced vibration tests to extract 18 flutter derivatives of the Hardanger Bridge cross-section. The new experimental setup is further used to simulate a three-degree-of-freedom dynamic system driven by white noise to investigate whether the estimates of the aerodynamic derivatives are sensitive to the motion considered. The experimental results demonstrate that the estimates of the aerodynamic derivatives are not sensitive to the motion considered; these results indicate that the principle of superposition is fully applicable for the cross section as long as the motions are within the range considered.

Keywords: Aerodynamic derivatives; Wind tunnel tests; Forced vibration technique; Narrow banded motion; Bridge aerodynamics.

1. Introduction

Wind-induced dynamic response is a critical concern when designing long-span bridges. In particular, instability phenomena, such as galloping and flutter, caused by the self-excited forces have received considerable attention in recent decades. Wagner (Fung 1955) and (Theodorsen (1935) developed analytical expressions for the self-excited forces of thin airfoils as early as 1925 and 1935, respectively. Bridge deck cross-sections are characterized by more complex geometrical shapes and flow patterns, which precludes the formulation of similar mathematical expressions (Kareem and Wu, 2014). Another approach is to use computational fluid dynamics to simulate the flow around a bridge section (e.g. Huang et al., 2009; Sarwar et al., 2008; Zhu et al., 2007); however, it still remains challenging to obtain reliable results, thus making wind tunnel testing necessary. Wind tunnel tests are commonly conducted using full bridge models, taut strip models or section models. Comparative studies of the performance of the approaches have been presented by Scanlan et al. (1997) and Wardlaw (1980). Section models are the most widely used (Diana et al., 2013; Ge and Xiang, 2008; Zasso et al., 2014) because the tests can be performed in reasonably sized wind tunnels and because it is possible to perform the tests at a larger scale (Matsuda et al., 2001; West and Apelt, 1982; Zasso et al., 2014). However, taut strip and full bridge models are commonly used to evaluate the overall performance of new bridge concepts, stretching the present state of the art, because it is possible to include several vibration modes in the modeling.
Despite the considerable progress made in the modeling of self-excited forces using rational or indicial functions (e.g. Cao and Sarkar, 2012; Caracoglia and Jones, 2003; Chowdhury and Sarkar, 2005; Costa, 2007; Costa and Borri, 2006; Salvatori and Borri, 2007; Zhang et al., 2011; Zhang and Chen, 2010; Øiseth et al., 2011, 2012), aerodynamic derivatives, as introduced in bridge engineering by Scanlan and Tomko (1971), remains the most common output from wind tunnel tests of bridges. The aerodynamic derivatives for a bridge cross-section can be determined by either forced or free vibration tests. In a free vibration test, the section model is suspended in springs and moves because of the initial conditions and mutual interactions between the wind flow and model.

In contrast, a prescribed motion of the bridge deck independent of the aerodynamic forces is considered in a forced vibration test. The section model is typically forced in either vertical, torsional or horizontal harmonic oscillations or combinations thereof. Thus, free vibration tests are considered to provide more realistic in-wind motion of the bridge deck and are easier to perform and less expensive; however, it is far more challenging to identify the aerodynamic derivatives from free vibration data; see (Bogunović Jakobsen and Hjorth-Hansen, 1995; Brownjohn and Jakobsen, 2001; Chowdhury and Sarkar, 2003; Sarkar et al., 1994; Scanlan, 1978) for an overview of the methodology available. The forced vibration technique provides higher data reliability (Diana et al., 2015) and is more suitable for higher velocities, larger motion amplitudes and higher turbulence intensities (Cao and Sarkar, 2012; Sarkar et al., 2009). However, the ability to consider a realistic bridge deck motion might be important for some cross sections. This consideration is reasonable because there are indications that the identification of the aerodynamic derivatives depends on the forced motion. For example, the aerodynamic derivatives have been shown to be influenced by the amplitudes of the motion (Chen et al., 2005; Scanlan, 1997), the frequency ratio between the torsional and vertical frequencies (Qin et al., 2009), and the effects of coupling between different degrees-of-freedom (DOFs) (Matsumoto et al., 1993). These findings indicate the importance of investigating when the current linear model is valid and when more complex nonlinear models should be applied.

This paper presents a new experimental setup that has potential to shed light on the underlying mechanisms of wind-induced forces by forcing the section model in nearly any desired motion. A typically reported weak point of the forced vibration technique is that induced vibrations are somehow different from those that the bridge will encounter in natural wind (Zhu et al., 2007). This enhanced rig overcomes this problem and enables aeroelastic forces to be measured directly when considering motions commonly observed in free vibration experiments. The herein described setup is used to investigate the accuracy of the assumptions frequently introduced to estimate aerodynamic derivatives from free vibration data; for example, the response is very narrow banded (Andersen et al., 2015; Brownjohn and Jakobsen, 2001) rather than being purely harmonic to obtain one reduced velocity. In this paper, the new experimental rig is first used to identify the full set of 18 aerodynamic derivatives for the Hardanger Bridge by performing standard forced vibration tests. Then, a random motion obtained by simulating a dynamic system driven by white noise is considered in the second round of tests. Finally, experimental results considering several frequency ratios are compared to the results obtained using a standard procedure to investigate whether the estimates of the aerodynamic derivatives are sensitive to the motion considered.

2. An enhanced forced vibration rig

Aerodynamic derivatives can be determined by moving a section model of the bridge deck in a prescribed motion while measuring the aerodynamic forces. Significant progress has been made since Ukeguchi et al., (1966) presented the first experimental results for bridge decks in 1966, and an impressive amount of forced vibration rigs used in research can be found in the literature (e.g. Cao and Sarkar, 2012; Chen et al., 2005; Diana et al., 2004, 2010, 2015; Falco et al., 1992; Han et al., 2014; Lee and Kwon, 2009; Li, 1995; Matsumoto et al., 1993; Matsumoto, 1996; Neuhaus et al., 2009; Sarkar et al., 2009). Forced vibration tests considering vertical and pitching motions are now routinely conducted when designing bridges, occasionally allowing for coupling between the two motions (Cao and Sarkar, 2012; Diana et al., 2004; Falco et al., 1992; Han et al., 2014). Several experimental setups capable of forcing the section model in horizontal, vertical and pitching motions have been presented more recently (Diana et al., 2004; Han et al., 2014; Lee and Kwon, 2009; Neuhaus et al., 2009; Sarkar, et al., 2004). It is interesting that experimental setup developed at Iowa State University (Cao and Sarkar, 2012; Sarkar et al., 2007, 2004) is able to perform both free and forced vibration test. It is achieved by a system of springs and pneumatic bushings that glide along polished steel shafts making the friction very low. Forced vibrations tests can the readily be performed by rods that are connected to the driving mechanism placed above the test section. The majority of the setups rely on a fixture of the section model sliding on linear rails that are driven by an eccentric shaft (Chen et al., 2005; Han et al., 2014; Li, 1995; Matsumoto et al., 1993; Neuhaus et al., 2009; Sarkar et al., 2007), whereas some setups are driven by electric or hydraulic actuators (Diana et al., 2004; Lee and Kwon, 2009). The forced vibration setups has advanced impressively regarding both forced frequencies and amplitudes (Neuhaus et al., 2009). Furthermore, the setups can also adapt a fluid medium instead of air to improve the accuracy of the force measurements (Li, 1995), enable the section model to be tested under different angles of attack or yaw angles (Diana et al., 2004) or generate impulsive step motion to be

generated to study the step response of the self-excited forces (Caracoglia and Jones, 2003). However, the continuous motion of the section in the forced vibration technique has been restricted to sinusoidal motions, which do not reflect the real bridge behavior. To amend this restriction, a new experimental setup was developed to test bridge deck section models in the forced vibration method. A strict requirement was that the forced vibration setup had to be capable of forcing the section model in an arbitrary motion to enable general-purpose section model tests. An image of the resulting machinery is shown in Fig. 1.

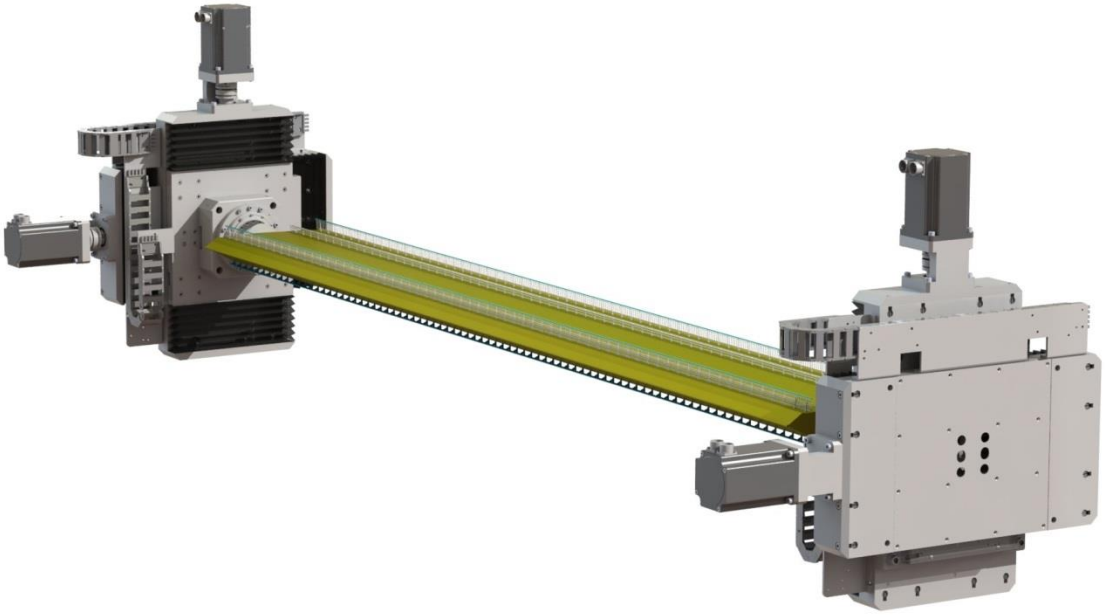

Fig. 1. New experimental forced vibration rig: section model mounted between the two actuators.

The forced vibration device consists of two 3-DOF actuators. These actuators are comprised of two linear motion slides on each side of the wind tunnel driven by ball screws that move the section model in the vertical and horizontal directions. Zero backslash shaft couplings connect the ball screws to servomotors and a servo motor with a planetary gear having a 1:50 gear ratio drives the torsional motion. The horizontal and vertical axes can travel ±10 cm, and the torsional axes can travel ±90 degrees. A customized multi-axis modular control system (MC4U from ASC Motion Control) is used to control the servomotors. The controller consists of two four axis servo drives, a 230 V, 8 kW power supply and a SPiiPlus motion controller. The servo processor receives the motion profile from the controller and then executes the real-time control algorithms at 20 kHz. The motion control system generates third-order motion profiles, making the acceleration and velocity linear and quadratic, respectively. This ensures that the motion is smooth, as presented in Fig. 2, where a random motion history is shown. The servo motors have been sized to handle large forces, making it easy to follow the motion profile for typical section models.

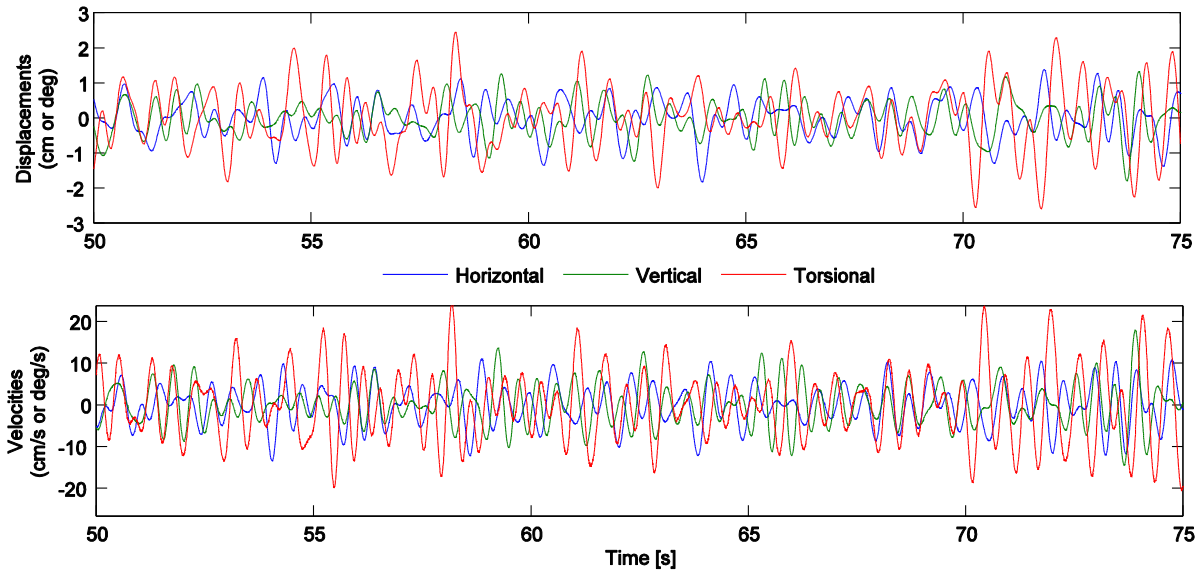

Fig. 2. Time series showing the measured motion of the section model when considering a random time series as input.

Two Gamma load cells supplied by ATI Industrial automation are used to measure three forces and three moments at each end of the section model. The six-axis force/torque transducers are placed between the section model and actuator, as shown in Fig. 3. Each load cell is bolted to the stage while a clamp is designed to attach the section model to the load cell. Similar solutions for force measurements were also used by Cigada et al., (2001), Han et al. (2014) and Körlin and Starossek (2007).

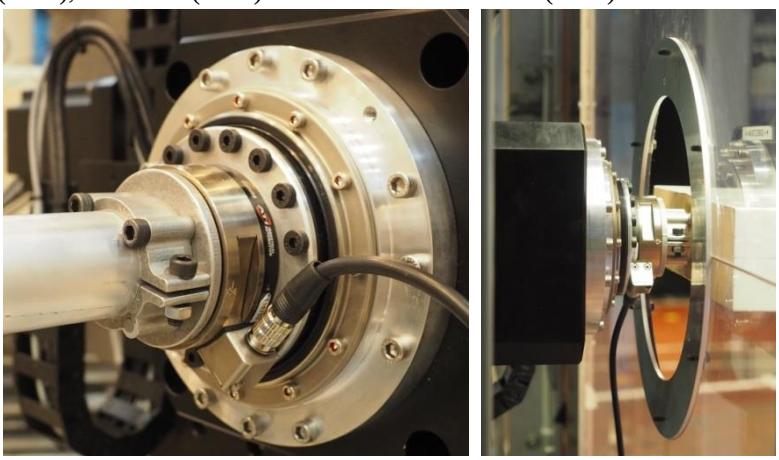

Fig. 3. Photograph showing how the section model is mounted to the load cell.

A flow chart of the experimental setup is shown in Fig. 4. As indicated in the Fig. 4, LabVIEW is used to control the experiment. The experiment starts by uploading a motion history to the MC4U controller. The controller communicates with the servo drives and ensures that the stages follow the motion profiles and that the actuators at both sides of the wind tunnel move synchronously. NI 9205 and NI 9239 analog input modules inserted into a NI cDAQ-9178 acquire the voltage signals from the load cells and the pressure transducer, and the LabVIEW program acquires the current position and velocity of the section model directly from the encoders on the servomotors using Ethernet communication via the MC4U controller. The sampling rate for the data acquisition was set to 250 Hz, and a time step of 1 ms was used for the uploaded motion time series.

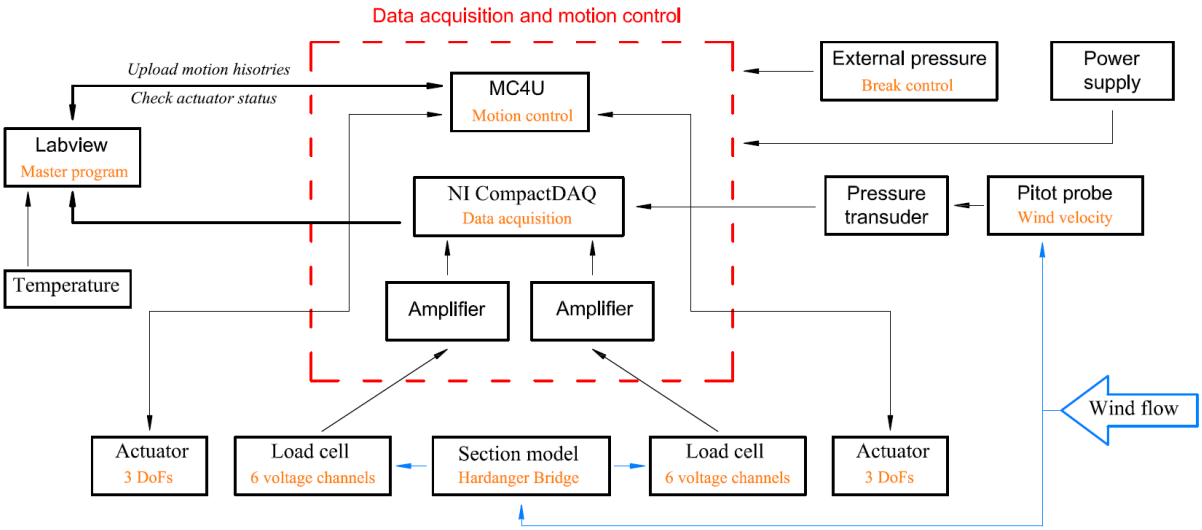

Fig. 4. Flowchart describing the data acquisition and motion control.

3. Identification of the aerodynamic derivatives from forced vibration tests

The self-excited forces for bridge decks are most commonly represented by aerodynamic derivatives, as suggested by Scanlan and Tomko (1971). The model defines unsteady self-excited aerodynamic forces for a section in single harmonic motion as

$$
\begin{aligned}
q_x^{Se} &= \frac{1}{2}\rho V^2 B\left(KP_1^* \frac{\dot{r}_x}{V} + KP_2^* \frac{B\dot{r}_\theta}{V} + K^2 P_3^* r_\theta + K^2 P_4^* \frac{r_x}{B} + KP_5^* \frac{\dot{r}_z}{V} + K^2 P_6^* \frac{r_z}{B} \right) \\
q_z^{Se} &= \frac{1}{2}\rho V^2 B\left(KH_1^* \frac{\dot{r}_z}{V} + KH_2^* \frac{B\dot{r}_\theta}{V} + K^2 H_3^* r_\theta + K^2 H_4^* \frac{r_z}{B} + KH_5^* \frac{\dot{r}_x}{V} + K^2 H_6^* \frac{r_x}{B} \right) \\
q_\theta^{Se} &= \frac{1}{2}\rho V^2 B^2\left(KA_1^* \frac{\dot{r}_z}{V} + KA_2^* \frac{B\dot{r}_\theta}{V} + K^2 A_3^* r_\theta + K^2 A_4^* \frac{r_z}{B} + KA_5^* \frac{\dot{r}_x}{V} + K^2 A_6^* \frac{r_x}{B} \right)
\end{aligned}
\tag{1}
$$

Here, V is the mean wind velocity; ρ is the air density; B is the width of the cross-section; $K=B\omega/V$ is the reduced frequency of motion, and r_x, r_z, and r_θ represent the horizontal, vertical and torsional displacements, respectively, that are defined positive as shown in Fig. 5. P_n^*, H_n^*, and A_n^* $n \in \{1, 2, \ldots 6\}$ are the dimensionless aerodynamic derivatives, which are assumed to be cross-sectional properties as functions of the reduced frequency. Eq. (1) is only valid for a single harmonic motion, but the self-excited forces for a more general motion can be obtained under the assumption that the principle of superposition holds.

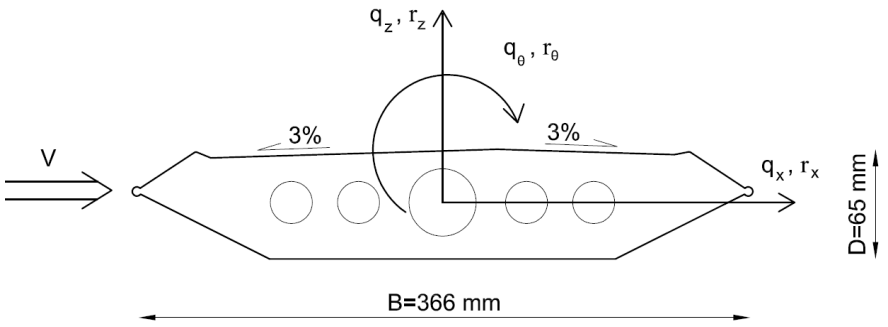

Fig. 5. Aerodynamic forces acting on the section model of the Hardanger Bridge.

There are several alternative methods for identifying aerodynamic derivatives from forced vibration test data. The aerodynamic derivatives are commonly determined from forced vibration tests by studying the phase angle between the self-excited forces and the motion of the section (Lee and Kwon, 2009; Matsumoto, 1996; Matsumoto et al., 1993; Neuhaus et al., 2009; Sarkar et al., 2009, 2007). Another option is to consider the complex Fourier amplitudes of the self-excited forces and how these are related to the aerodynamic derivatives;

see (Chen et al., 2005; Li, 1995; Siedziako et al. 2016) for further details. These techniques are straightforward, but as noted by Cao and Sarkar (2012) and Neuhaus et al. (2009), they can result in significant estimation errors in certain cases because of the uncertainties in the estimate of the phase angle or, as reported by Han et al. (2014), because of spectral leakage caused by the frequency domain truncation. A better approach is perhaps to use a time domain method, where the model for the self-excited forces is fitted to the time series of the self-excited forces by least squares, as suggested by Han et al. (2014). An extended version of this method that can consider a more complex motion was recently developed by (Siedziako et al. 2016). By rewriting Eq. (1), the self-excited forces can be expressed as follows:

$$\mathbf{q}_{Se}(t,K,V) = \mathbf{XE} \tag{2}$$

Here, $\mathbf{q}_{\mathrm{Se}}$ (t,K,V) represents the self-excited forces; the coefficient matrix **E** containing the aerodynamic derivatives and the matrix **X** containing the motion histories are defined below.

$$\mathbf{E} = \frac{1}{2}\rho V^2 B \begin{bmatrix} K_y P^*_1 / V & K_y H^*_5 / V & BK_y A^*_5 / V \\ K_z P^*_5 / V & K_z H^*_1 / V & BK_z A^*_1 / V \\ BK_\theta P^*_2 / V & BK_\theta H^*_2 / V & B^2 K_\theta A^*_2 / V \\ K_y^2 P^*_4 / B & K_y^2 H^*_6 / B & K_y^2 A^*_6 \\ K_z^2 P^*_6 / B & K_z^2 H^*_4 / B & K_z^2 A^*_4 \\ K_\theta^2 P^*_3 & K_\theta^2 H^*_3 & BK_\theta^2 A^*_3 \end{bmatrix} \tag{3}$$

$$\mathbf{X} = \begin{bmatrix} \dot{r}_{\mathrm{x},1} & \dot{r}_{\mathrm{z},1} & \dot{r}_{\theta,1} & r_{x,1} & r_{\mathrm{z},1} & r_{\theta,1} \\ \dot{r}_{\mathrm{x},2} & \dot{r}_{\mathrm{z},2} & \dot{r}_{\theta,2} & r_{x,2} & r_{\mathrm{z},2} & r_{\theta,2} \\ \vdots & \vdots & \vdots & \vdots & \vdots & \vdots \\ \dot{r}_{\mathrm{x,n}} & \dot{r}_{\mathrm{z,n}} & \dot{r}_{\theta,\mathrm{n}} & r_{\mathrm{x,n}} & r_{\mathrm{z,n}} & r_{\theta,\mathrm{n}} \end{bmatrix} \quad q_{Se} = \begin{bmatrix} q_{Se,\mathrm{x},1} & q_{Se,\mathrm{z},1} & q_{Se,\theta,1} \\ q_{Se,\mathrm{x},2} & q_{Se,\mathrm{z},2} & q_{Se,\theta,2} \\ \vdots & \vdots & \vdots \\ q_{Se,\mathrm{x,n}} & q_{Se,\mathrm{z,n}} & q_{Se,\theta,\mathrm{n}} \end{bmatrix} \tag{4}$$

The coefficient matrix **E** and thus the aerodynamic derivatives are obtained by minimizing the sum of squares.

$$\mathbf{E} = (\mathbf{X}^{\mathrm{T}}\mathbf{X})^{-1}\mathbf{X}^{\mathrm{T}}\mathbf{q}_{Se} \tag{5}$$

The aerodynamic derivatives are determined by a least squares fit to the time series of the measured self-excited forces using the approach above. A least squares fit to recorded time series has also been used by Cao and Sarkar (2012) to determine the coefficients defining Rational Functions and by Chowdhury and Sarkar (2003) to identify aerodynamic derivatives from free vibration tests.

4. Wind Tunnel Tests

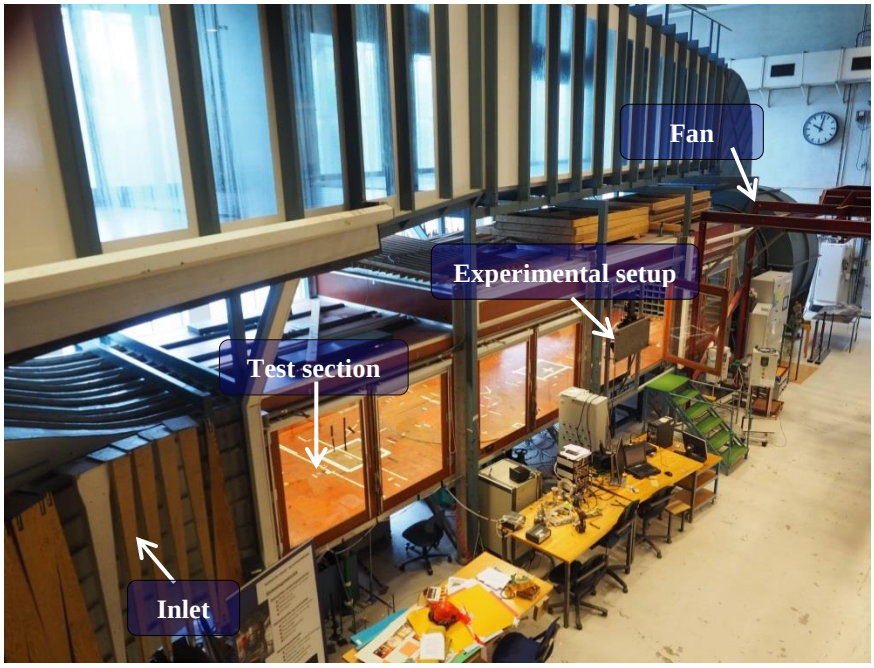

Fig. 6. Wind tunnel used in this study.

The experiments were conducted in one of the wind tunnels in the Fluid Mechanics Laboratory at the Norwegian University of Science and Technology. The wind tunnel is a low-speed, closed loop with an 11 m-long, 2 m-high and 2.7 m-wide test section. A picture of the wind tunnel is shown in Fig. 6, where the essential components are highlighted. A 220 kW motor drives the fan, which can generate a maximum wind speed of 30 m/s. The velocity profile at the inlet is uniform, and the flow is close to laminar, with a turbulence intensity of approximately 0.2% (Adaramola and Krogstad, 2009). A photograph of the section model mounted between the load cells is shown in Fig. 7. The actuators are mounted outside the wind tunnel, and the load cells are placed in the center of two circular holes with a diameter of 25 cm. End plates are deemed not required because the clearance between the ends of the section model and the wind tunnel walls was only 1.5 cm; see Fig. 3 for more details. The section model has a high aspect ratio (L/B=7.32) in order to ensure predominantly two-dimensional flow. The pitot probe was placed 2.15 m from the wind tunnel inlet and 6.1 m in front of the section model. The temperature varied between 20 and 24°C during the experiments, which was considered when calculating the wind speed by considering how the air density varies with temperature.

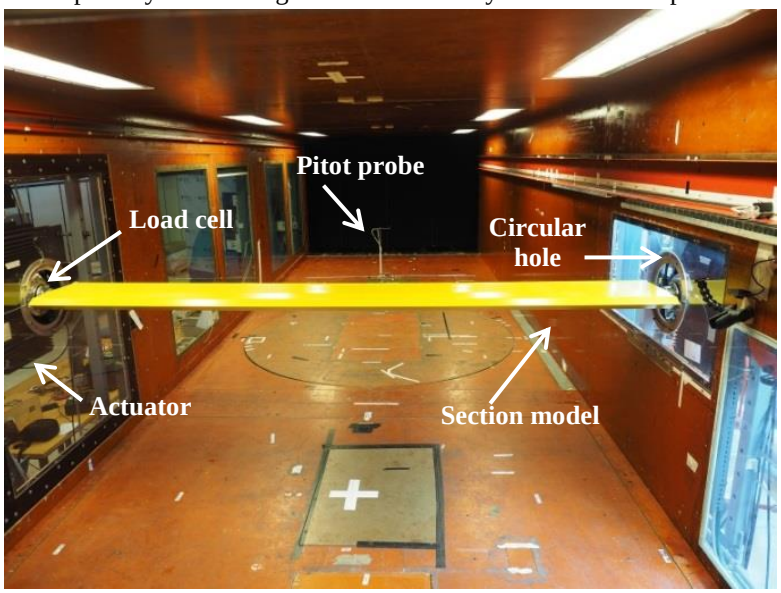

Fig. 7. Section model installed in the wind tunnel. The actuators are placed outside the wind tunnel.

4.1. Section model

A section model of the Hardanger Bridge, which was studied extensively at NTNU (Øiseth et al., 2010; Øiseth et al., 2012), is considered in this study. Currently, there is a comprehensive monitoring system installed on the site (Fenerci and Øiseth, 2015; Øiseth et al., 2015); this system can provide further insight into the aerodynamic behavior of the bridge deck. The corresponding section model was produced at a scale of 1:50, giving the dimensions presented in Fig. 5. The model consists of an aluminum pipe with an outer diameter of 40 mm and a wall thickness of 1 mm that provides the majority of the stiffness. The main geometry of the section was milled in two parts, which were glued onto the pipe. The model was milled in Gurit PVC60 to make it as light as possible, and the four cylindrical cavities were made to reduce the mass. The railings and guide vanes were 3D printed. The surface of the section model was hardened with a thin layer of synthetic paint. The final section model is 2.68 m long and has a mass of only 5.45 kg. The lowest natural frequency of the model is 12 Hz, which is considered to be sufficiently high to avoid dynamic amplification in the frequency range of interest.

Fig. 8: Photographs illustrating the production of the section model.

4.2. Obtaining the self-excited forces from the measured forces

The time histories of self-excited forces must be available to identify aerodynamic derivatives using Eq. (5). However, the self-excited forces are only a part of the total forces recorded by the load cells during the tests. The total forces acting on the section model can be expressed as

$$\mathbf{Q}_{tot}(\mathbf{r},\dot{\mathbf{r}},\ddot{\mathbf{r}},\mathrm{V},u,\mathrm{w}) = \mathbf{Q}_G + \mathbf{Q}_I(\ddot{\mathbf{r}}) + \mathbf{Q}_B(\mathrm{V},u,w) + \mathbf{Q}_{Se}(\mathrm{V},\mathbf{r},\dot{\mathbf{r}}) + \mathbf{Q}_S(\mathrm{V}) \tag{6}$$

Here, the vector $\mathbf{Q}_{tot}(\mathbf{r},\dot{\mathbf{r}},\ddot{\mathbf{r}},\mathrm{V},u,\mathrm{w})$ denotes the total forces, $\mathbf{Q}_G$ is the static load due to the self-weight of the model, $\mathbf{Q}_I(\ddot{\mathbf{r}})$ is the inertia forces, and $\mathbf{Q}_B(u,w)$, $\mathbf{Q}_{Se}(\mathbf{r},\dot{\mathbf{r}})$, and $\mathbf{Q}_S(\mathrm{V})$ denote the buffeting forces, self-excited forces and mean wind forces, respectively. The horizontal and vertical turbulence components are denoted as u and w, respectively. The time-invariant forces can be deleted by simply removing the mean value of the measured forces; the buffeting forces can be neglected because the experiments are conducted in smooth flow, whereas the inertia forces must be considered and properly evaluated. There are three different methods to remove the inertia forces from the time series. The simplest approach is to remove the contribution from inertia relying on the acceleration time histories, the measured mass of the section model and the estimated mass moment of inertia. This method is rather inaccurate and is thus not recommended. Another alternative is to measure the forces for the same motion histories that are applied in the wind tunnel tests in still-air. The recorded still-air time series can then either be subtracted directly from the in-wind time series or used to identify the mass matrix of the section model more accurately. The last two methods have been termed "Wind-NoWind" and "Wind-InertialForce" and were compared by Diana et al. (2004). The "Wind-InertialForce" approach is only appropriate for the diagonal terms in the aerodynamic stiffness and damping matrices ($P_{1,4}^*$, $H_{1,4}^*$, and $A_{2,3}^*$). Thus, the "Wind-No Wind" approach was applied in this study.

5. Experimental results and discussion

5.1. Standard forced vibration tests

Although the experimental setup presented herein is capable of forcing arbitrary motion histories, we started by identifying the aerodynamic derivatives of the Hardanger Bridge using the standard procedure. The section model is then forced into vertical, horizontal, or torsional harmonic motions separately to obtain all 18 aerodynamic derivatives. The amplitudes, frequencies and wind velocities tested are listed in Table 1. This

implies that a total of 4×7×3=84 time series were used to obtain 84/3=28 data points for each of the aerodynamic derivatives.

Amplitude of the vertical vibrations	1.5 cm	Tested velocities	4, 8, 10 and 12 m/s
Amplitude of the horizontal vibrations	1.5 cm	Tested frequencies	0.5, 0.8, 1.1, 1.4, 1.7, 2.0 and 2.5 Hz
Amplitude of the torsional vibrations	2°	Reduced velocity range	From 0.7 up to 10.4
Sampling frequency	250 Hz	Duration of the time series	50 seconds

Table 1. Overview of the frequencies and amplitudes considered in the standard forced vibration tests

The identified aerodynamic derivatives and a third-order polynomial fit to the data together with corresponding confidence intervals are shown in Fig. 9 and Fig. 10. The confidence bounds have been obtained based on the least squares fit of the polynomial coefficients to the data points using standard Matlab functions. Different combinations of frequencies and velocities, as indicated by the marker types, provide data points at reduced velocities ranging from 0.7 up to 10.4. The experimental data show a clear trend, indicating that the self-excited forces can be characterized by the reduced velocity, as assumed by Scanlan and Tomko (1971). The confidence bounds nearly overlap with the polynomial fit for the critical aerodynamic derivatives H_3, A_3, A_1 and A_2, whereas more scatter can be observed for the aerodynamic derivatives defining the self-excited drag force. This observation might be the result of the low magnitude of this force component compared to the inertia forces involved, which makes it difficult to obtain accurate time histories of the self-excited drag force using Eq. (6).
Wind tunnel tests of the Hardanger bridge was also performed as a part of the design of the bridge using buffeting free vibration technique (Bogunović Jakobsen and Hjorth-Hansen 1995; Svend Ole Hansen ApS 2009). The obtained aerodynamic derivatives from both tests are displayed in Fig. 11. It must be emphasized that a direct comparison is not possible as the geometry of the models slightly differ and the box girder tested herein was without any guide vanes or handrails, while handrails were included in the free vibration tests. Yet still, Fig 11 shows that the experimental results agrees very well, in particular when taking into consideration the geometrical dissimilarities that are known to have a significant impact on the aerodynamic derivatives, see for instance (Jones et al.,1995). The reliability of the new experimental setup was further assessed by comparing the predicted self-excited forces using the identified derivatives to the measured self-excited forces, as shown in Fig. 12. The correlation coefficient of the measured and predicted aeroelastic forces is used to evaluate the accuracy of the predictions. The correlation coefficients for all 84 tests are shown in Fig. 13. Every colored bar can be related to two aerodynamic derivatives; for example, A_1^* and A_4^* produce a pitching moment due to vertical motion. High correlation coefficients for the lift and pitch time histories are achieved when the section was rotating or moving vertically. The recorded self-excited forces were small in the case of horizontal motion, particularly at low wind velocities; however, the pitching moment and lift were still predicted relatively well. As noted above, the low magnitude of the self-excited drag force (typically below 0.1 N/m) is a possible reason for the low correlation coefficient between the measured and predicted forces, particularly when vertical motion is used. Another explanation can be deduced from recent studies by Xu et al. (2016), who observed the presence of higher-order self-excited drag force, while only the linear (frist-order) contribution can be captured with aerodynamic derivatives. However, as shown in Fig. 9 and Fig. 10, the shapes of P_1^*, P_4^*, H_5^*, H_6^*, A_5^*, A_6^* are still determined relatively well, indicating that the identification method outlined above is rather robust. Scatter in aerodynamic derivatives defining drag force can likely be lowered in this case by performing tests at higher wind speeds and amplitudes, using more sensitive load cells and taking into account nonlinear effects.

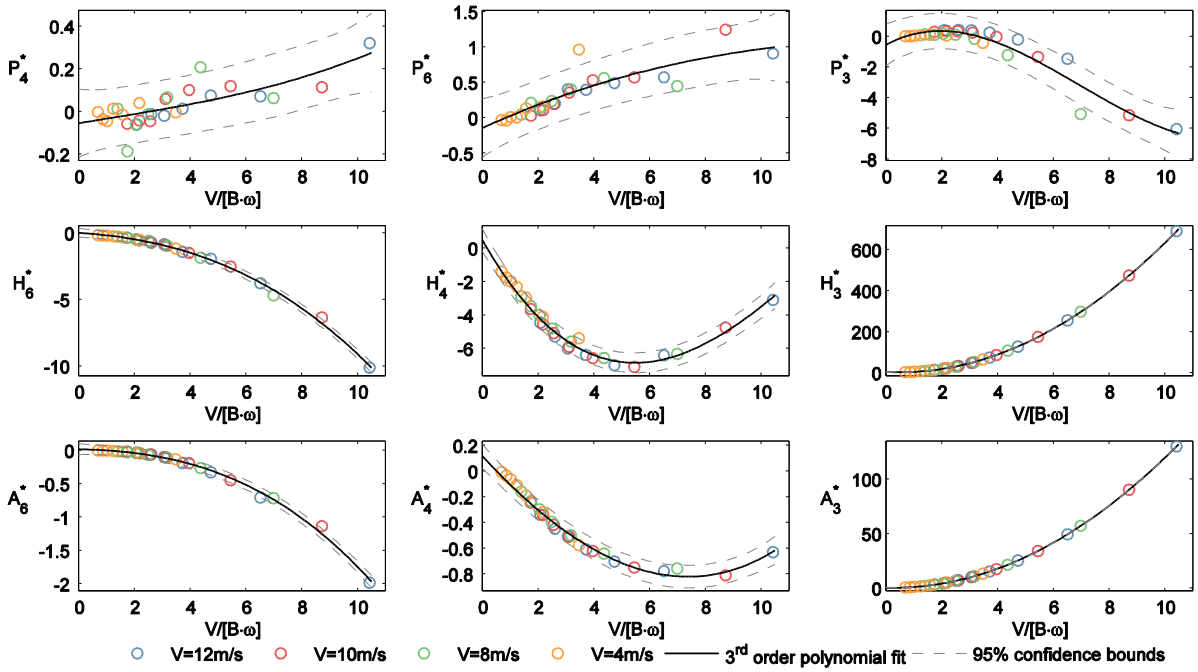

Fig. 9. Aerodynamic derivatives related to displacements or rotation.

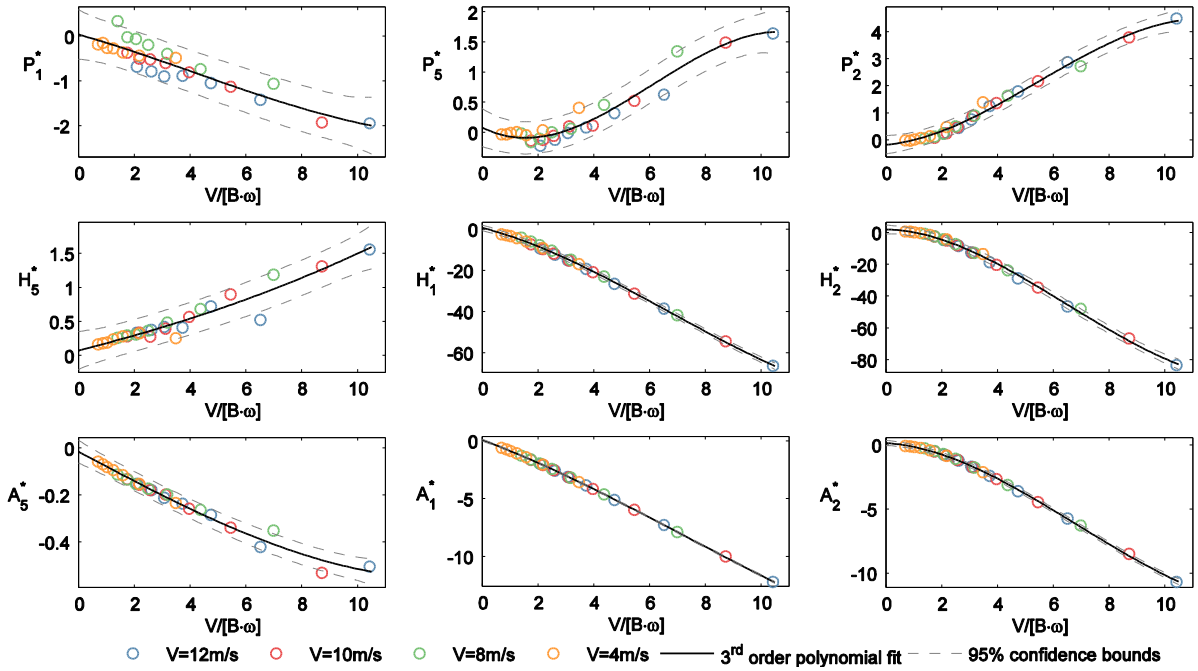

Fig. 10. Aerodynamic derivatives related to velocities or angular velocities.

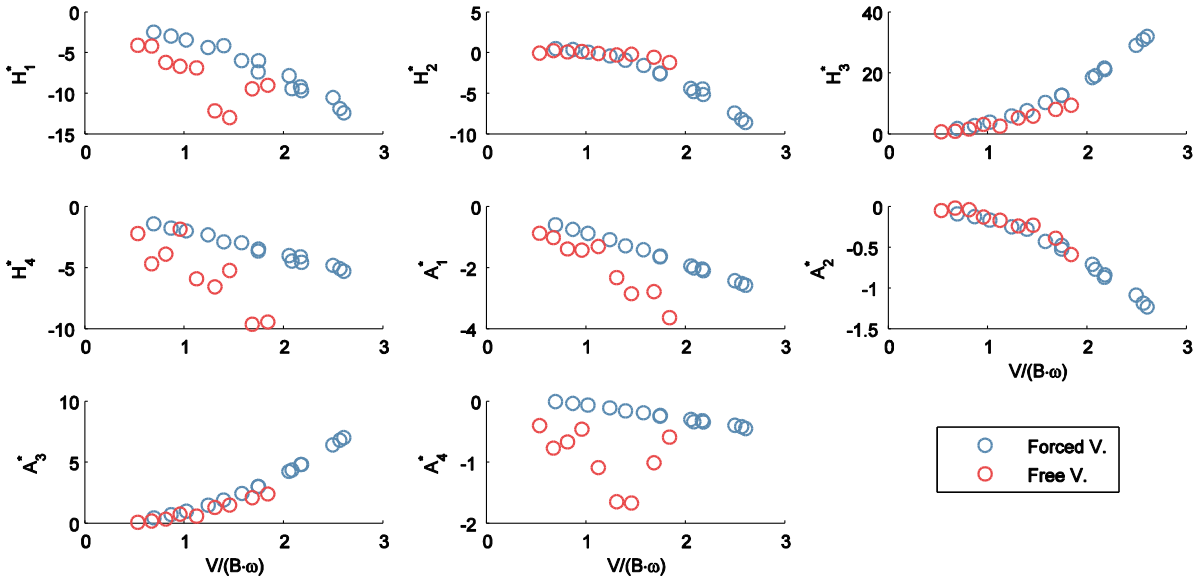

Fig. 11. Comparison of aerodynamic derivatives obtained with the forced vibration setup and free vibration 2 DOF tests. Note that no handrails were included in the forced vibration tests.

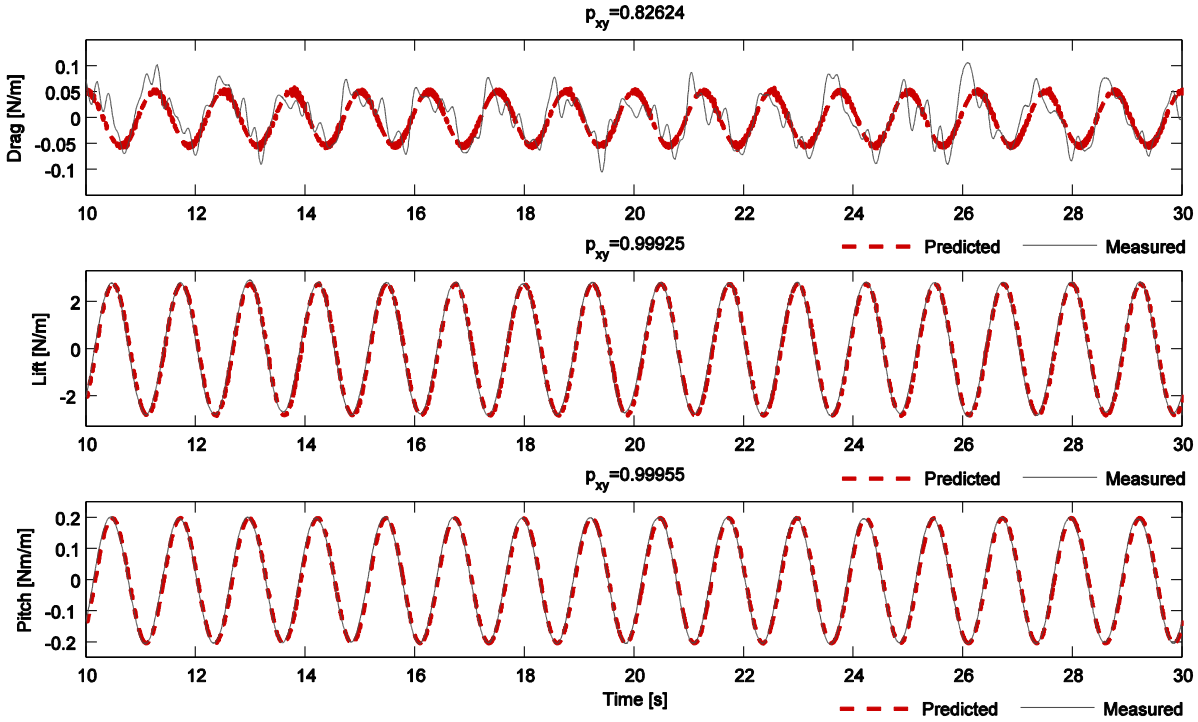

Fig. 12. Predicted vs measured drag, lift and pitching moment for a torsional motion with an amplitude of 2° and frequency of 0.8 Hz at V=8 m/s.

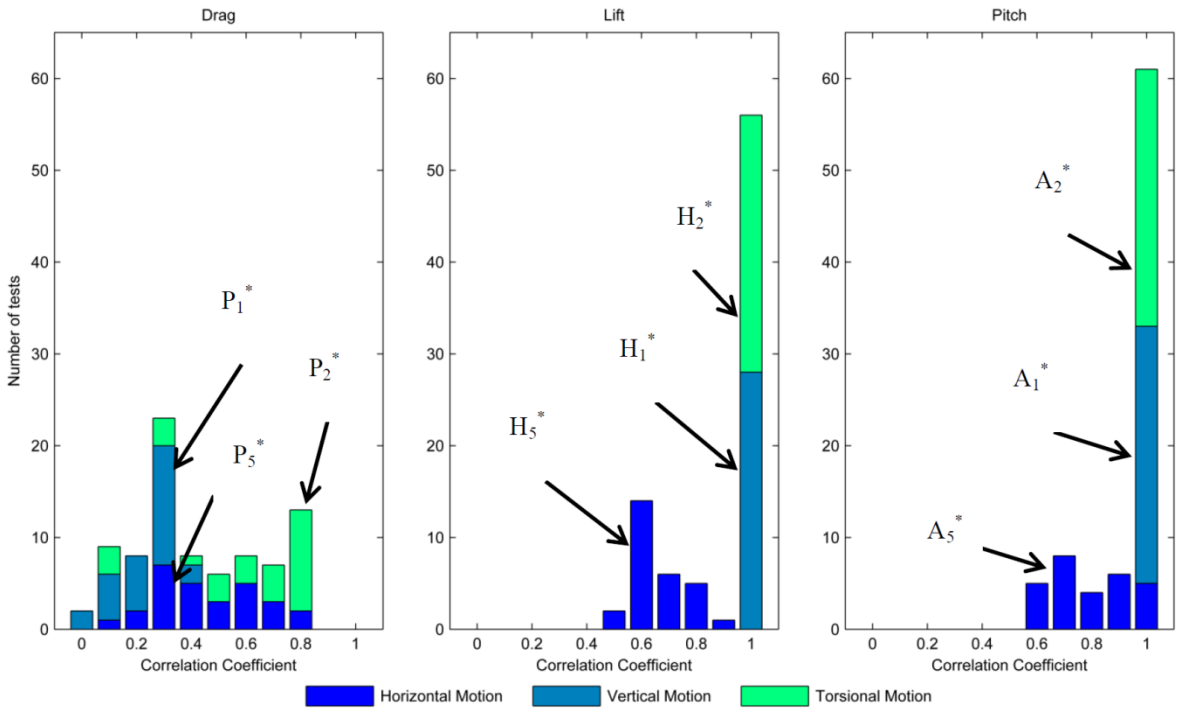

Fig. 13. Histograms of correlation coefficients between the measured and predicted self-excited forces.

5.2. Simulating a three-degree-of-freedom system

The standard forced vibration test outlined above does not resemble the motion of the actual bridge subjected to wind loading, which can be a weak point in the procedure if the model for the self-excited forces does not fully hold. In such cases, it is better to identify the aerodynamic derivatives of the bridge deck considering a motion that is similar to the actual motion of the bridge, which is one of the reasons why some researchers and bridge designers prefer free vibration tests even if the results are slightly more scattered than the results from forced vibration tests. The experimental setup outlined in section 1 makes it possible to perform forced vibration tests considering a motion that resembles the actual bridge motion. The applied motion is obtained by simulating a dynamic system with three degrees of freedom subjected to white noise. The cross-spectral density matrix of the response can be obtained by

$$\mathbf{S_r}(\omega) = \mathbf{H}(\omega)\mathbf{S_Q}(\omega)\mathbf{H}^*(\omega) \tag{7}$$

Here, $\mathbf{S_r}(\omega)$ is the cross-spectral density matrix of the response, $\mathbf{H}(\omega)$ represents the frequency response matrix of the system and $\mathbf{S_Q}(\omega)$ symbolizes the cross spectral density matrix of the load that is assumed as uncorrelated white noise $\mathbf{S_Q}(\omega) = \mathrm{diag}\left(\begin{bmatrix} S_y & S_z & S_\theta \end{bmatrix}\right)$. The amplitudes S_n, $n \in \{x, z, \theta\}$, are scaled such that the standard deviations of the horizontal, vertical and torsional responses are 5 mm, 5 mm and 0.95°, respectively. The time series of the motion is obtained by Monte Carlo simulations (Aas-Jakobsen and Strømmen, 2001; Kareem, 2008; Shinozuka, 1972; Shinozuka and Jan, 1972) with a cut-off frequency of ω_u=15 Hz and $\Delta\omega$=0.00001 rad/s. The time series for degree of freedom $m \in \{x, z, \theta\}$ can then be obtained by

$$x_m(t) = \sqrt{2\Delta\omega}\,\mathrm{Re}\left(\sum_{l=1}^{m}\sum_{k=1}^{N} L_{ml}(\omega_k)\exp\left(i(\omega_k + \phi_{lk})\right)\right) \tag{8}$$

Here, $L_{ml}(\omega_k)$ denotes the elements of the lower triangular matrix obtained by factorizing the cross-spectral density matrix according to the relation

$$\mathbf{S_r}(\omega_k) = \mathbf{L}(\omega_k)\mathbf{L}^*(\omega_k) \tag{9}$$

Because the resulting motion is a combination of horizontal, vertical and torsional motion, it is possible to obtain one data point for all 18 flutter derivatives from one test. The properties considered in the tests are listed in Table 2. The frequencies were chosen to reflect the typical frequency ratios for long-span bridges. The exception is test 4, where the frequency of the vertical vibration mode is higher than the frequency of the torsional vibration mode to investigate the presence of the vertical-to-torsional frequency ratio dependency observed, for example, by Qin et al. (2009) for a rectangular and twin deck sections. The auto spectral densities of the response and the realization of the response process for one of the test are presented in Fig. 14 and Fig. 15, respectively. The aerodynamic derivatives are still determined by applying Eq. (2) to (5). The time series generated from the assumed cross-spectral density matrix presented in Eq. (7). The forces have been measured for motion in still-air and in-wind conditions following the standard forced vibration procedure outlined above. However, one must assume that the aerodynamic derivatives are constant in a small region around the peak frequency and that the frequency components around the peaks in the response spectra dominates the self-excited forces, which is also assumed when identifying aerodynamic derivatives from the free vibration test. The duration of each test was taken as 360 s.

Test no.	Peak frequency			Tested wind velocities
	Horizontal	Vertical	Torsional	
Test 1	0.2 Hz	0.5 Hz	1.0 Hz	4, 8, 12 m/s
Test 2	0.2 Hz	0.5 Hz	2.0 Hz	4, 8, 12 m/s
Test 3	0.2 Hz	0.5 Hz	3.0 Hz	4, 8, 12 m/s
Test 4	0.2 Hz	2.0 Hz	0.5 Hz	4, 8, 12 m/s

Table 2. Natural frequencies of the dynamic system used to generate the time series of the 3-DOF system driven by white noise.

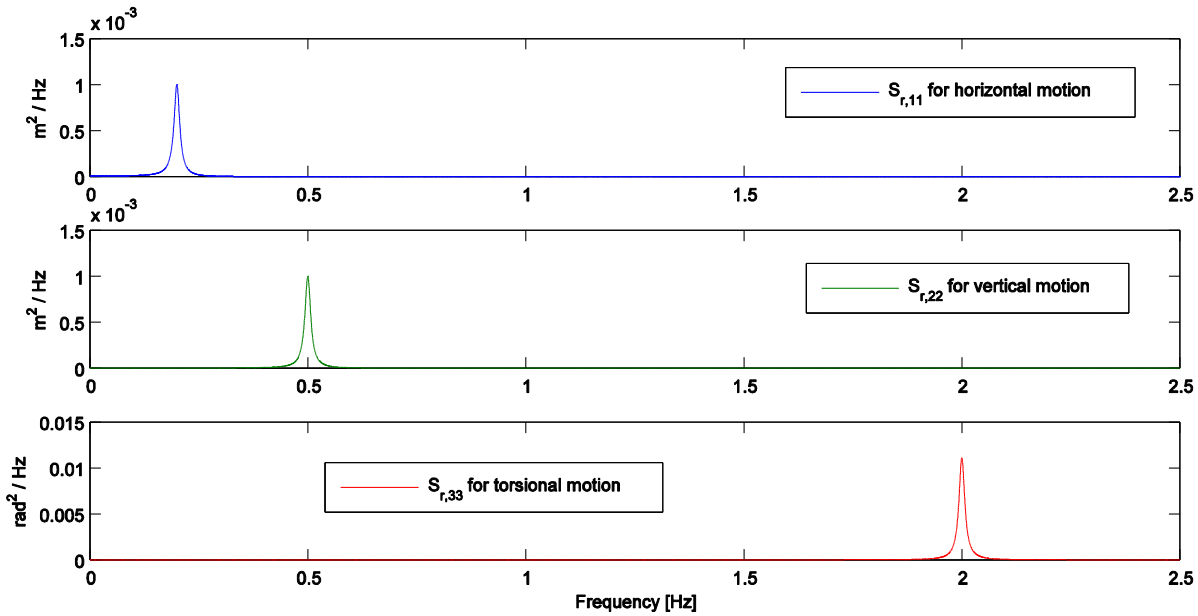

Fig. 14. Spectral densities used to generate the narrow banded time series used for test 2.

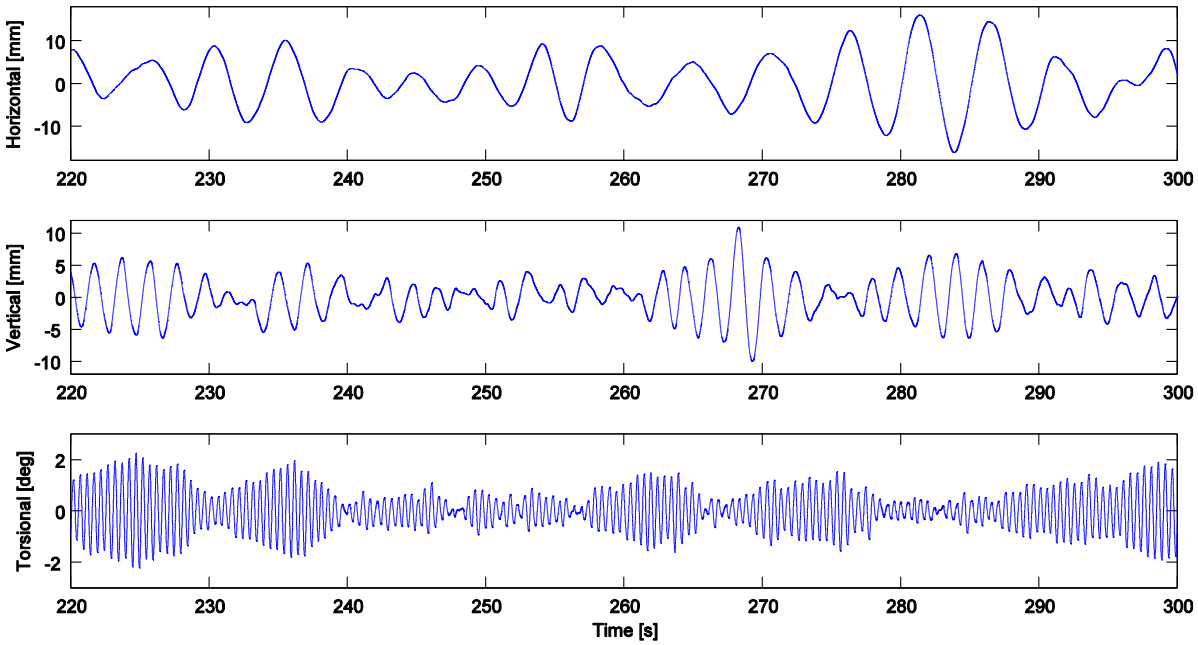

Fig. 15. Parts of the horizontal, vertical and torsional motion histories generated from narrow-banded spectra for test 2.

The resulting aerodynamic derivatives are shown in Fig. 16 and Fig. 17. The polynomial fit to the data from the standard forced vibration test together with the confidence intervals are also plotted to make it easier to identify any discrepancies. As seen, there are no significant discrepancies for the important aerodynamic derivatives. For aerodynamic derivatives related to torsional motion, P_3^*, P_2^*, H_3^*, H_2^*, A_3^*, and A_2^*, all the data points are within the confidence bounds of the results from the standard forced vibration test. For the aerodynamic derivatives related to vertical motion, there are significant discrepancies for P_5^* and P_6^* and some discrepancies for A_4^*. For the aerodynamic derivatives related to horizontal motion, H_6^*, A_6^* and P_1^* correspond well to the results from the standard test, whereas the results for P_4^*, H_5^* and A_5^* are severely scattered. However, it should be noticed that the last three mentioned aerodynamic derivatives have a minor influence on the total aeroelastic forces.

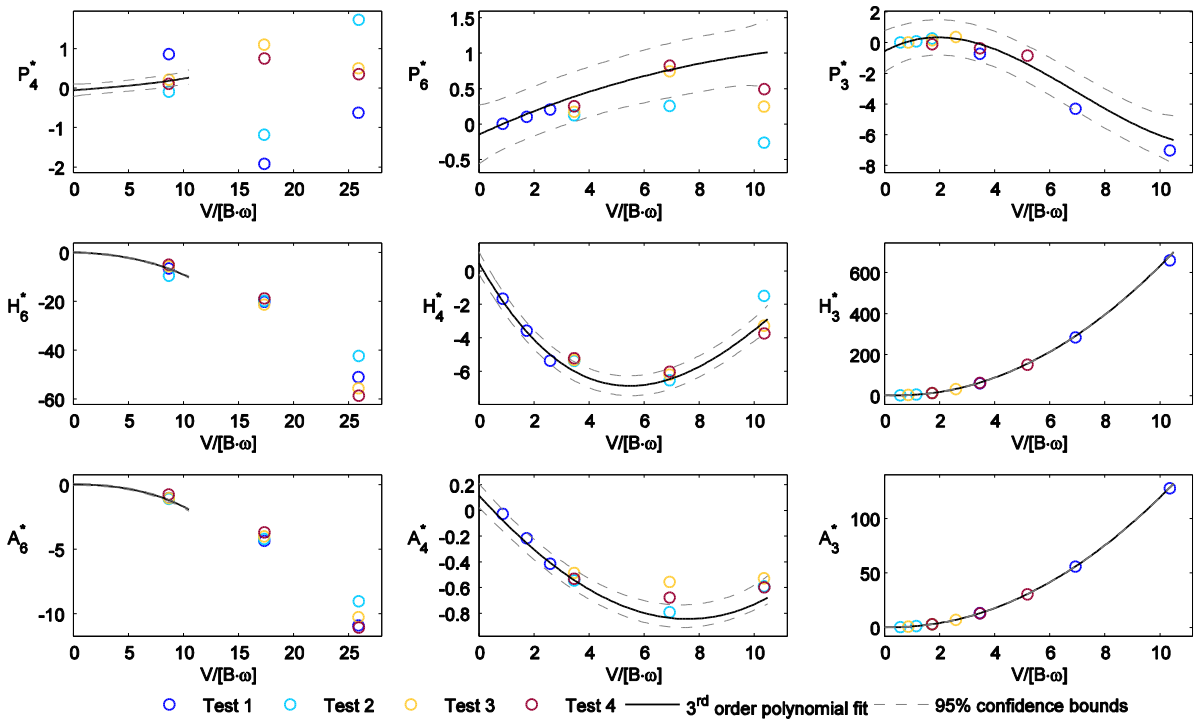

Fig. 16. Identified aerodynamic derivatives related to the displacements or rotations considering narrow-banded motion. The polynomial fit and confidence bounds from the standard forced vibration test are shown for comparison.

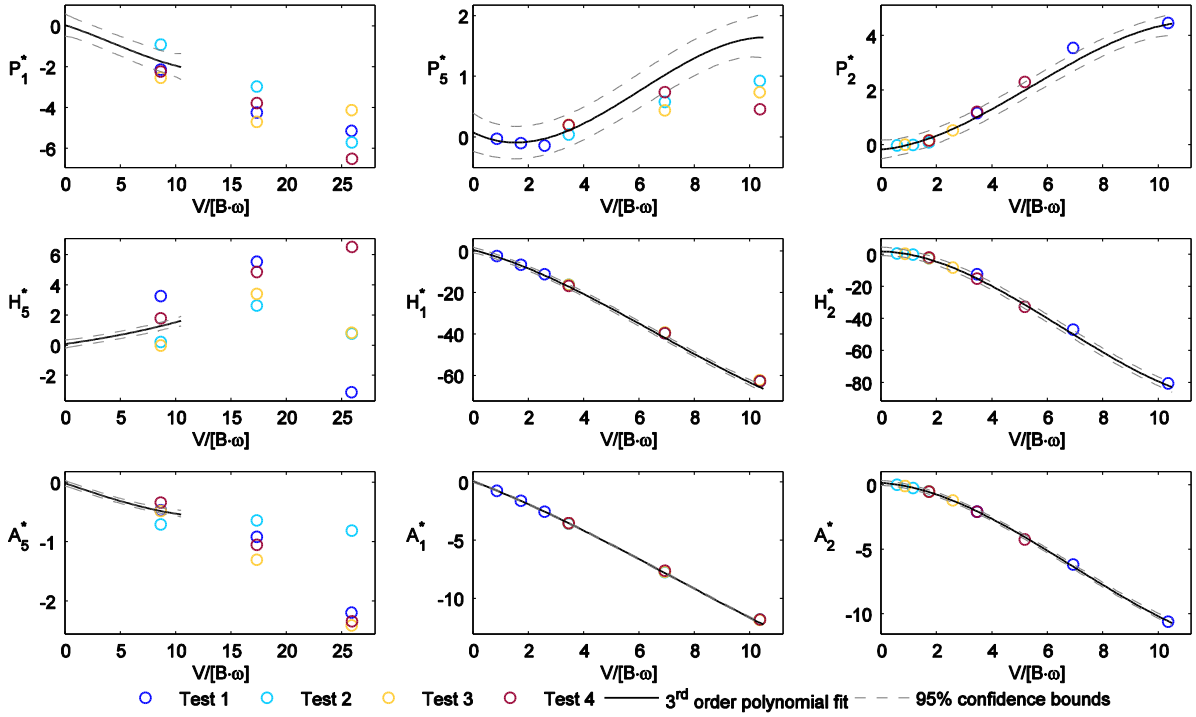

Fig. 17. Identified aerodynamic derivatives related to the velocities or angular velocities considering narrow-banded motion. The polynomial fit and confidence bounds from the standard forced vibration test are shown for comparison.

A typical example of the measured and predicted time histories of the self-excited forces is presented in Fig. 18. The self-excited forces were predicted for comparison using aerodynamic derivatives from the standard test (polynomial fit) as well as those presented in this section. The lift force and pitching moment predicted using

both sets of experimental data corresponds well to the measured lift force and pitching moment, and larger discrepancies were observed for the drag force. The self-excited drag force is small, making it challenging to measure and thus explaining the majority of the discrepancies observed.

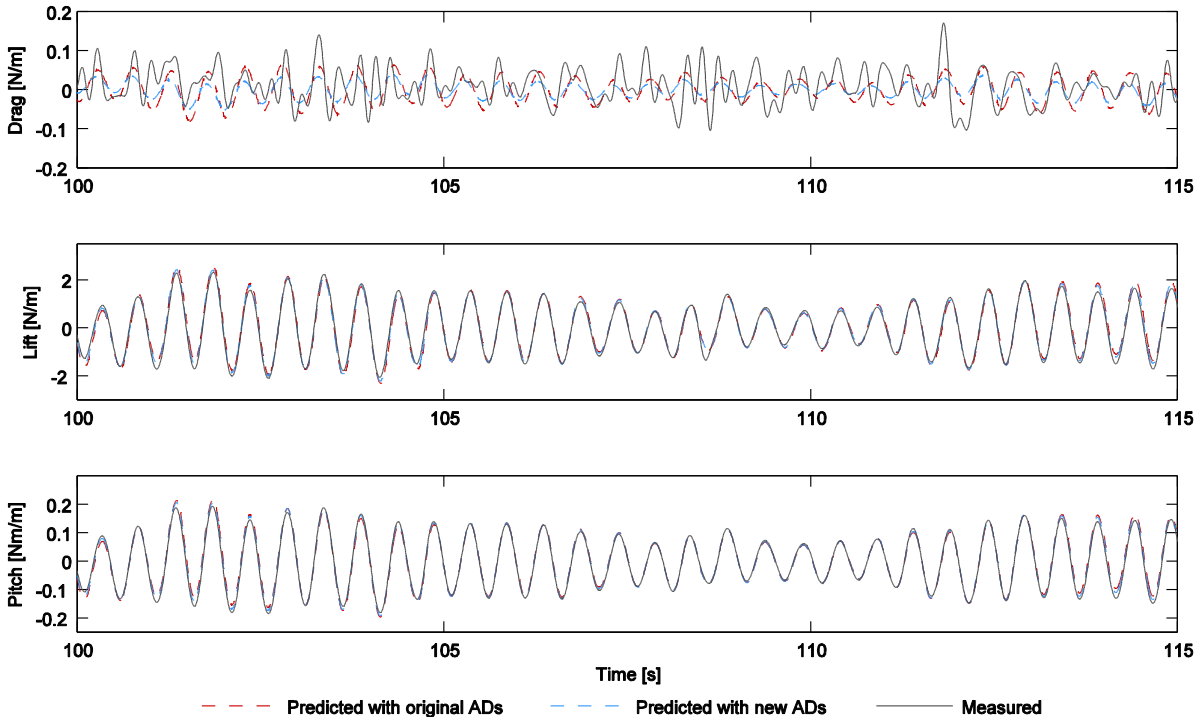

Fig. 18. Predicted vs. measured self-excited forces for test 2 at a mean wind velocity of 8 m/s.

6. Concluding remarks

This paper presented a new experimental setup capable of forcing section models in arbitrary horizontal vertical and torsional motion. The performance of the rig was first tested by identifying the full set of 18 aerodynamic derivatives for the cross section of the Hardanger Bridge using the standard forced vibration test procedure. The obtained aerodynamic derivatives showed little scatter and thus narrow confidence intervals for a wide range of reduced velocities. This result confirms that the described system is capable of forcing the section model in a smooth harmonic motion and that the aerodynamic derivatives capture the self-excited forces for the section model in an excellent manner. The low scatter can also partly be attributed to the procedure used to obtain the aerodynamic derivatives from the time series of the self-excited forces as well as method of extracting them from total recorded forces. A more general motion was further considered by tests simulating a 3-DOF dynamic system driven by white noise to replicate the typical motions observed in buffeting free vibration tests. This motion is of great interest because it is closer to the vibrations the bridge will encounter in strong winds. Several frequency ratios were considered to investigate whether the results are sensitive to the type of motion considered. The aerodynamic derivatives were obtained assuming that the response is narrow banded, which is a typical assumption when identifying the aerodynamic derivatives from free vibration tests. The obtained aerodynamic derivatives, considering all of the tested frequency ratios, correspond to the results using the standard forced vibration procedure nearly perfectly. Some discrepancies are observed for P_4^*, P_5^*, P_6^* and H_5^*; however, their influence on the self-excited forces is low, thereby making them difficult to identify accurately. The results indicate that the principle of superposition of different DOFs is fully applicable for the cross section tested and that the aerodynamic derivatives accurately predict the self-excited forces.

Acknowledgement

This research was conducted with financial support from the Norwegian Public Roads Administration. The authors gratefully acknowledge this support.

References

Aas-Jakobsen, K., Strømmen, E., 2001. Time domain buffeting response calculations of slender structures. Journal of Wind Engineering and Industrial Aerodynamics, 89(5), 341–364. http://doi.org/10.1016/S0167-6105(00)00070-2

Adaramola, M. S., Krogstad, P.-Å., 2009. Model Tests of a Horizontal Axis Wind Turbine in Yawed Condition. In European Offshore Wind Conference and Exhibition, Stockholm.

Andersen, M. S., Læsø, J. R., Lenius, M., & Johansson, J., 2015. Non-flutter design principle for twin boxes. In 14th International Conference on Wind Engineering, Porto Alegre.

Bogunović Jakobsen, J., Hjorth-Hansen, E.. 1995. Determination of the aerodynamic derivatives by a system identification method. Journal of Wind Engineering and Industrial Aerodynamics, 57, 295–305. http://doi.org/10.1016/0167-6105(95)00006-D

Brownjohn, J. M. W., Jakobsen, J. B., 2001. Strategies for aeroelastic parameter identification from bridge deck free vibration data. Journal of Wind Engineering and Industrial Aerodynamics, 89(13), 1113–1136.

Cao, B., Sarkar, P. P., 2010. Identification of Rational Functions by Forced Vibration Method for Time-Domain Analysis of Flexible Structures. In Proceedings of The Fifth International Symposium on Computational Wind Engineering, Chapel Hill.

Cao, B., Sarkar, P. P., 2012. Identification of Rational Functions using two-degree-of-freedom model by forced vibration method. Engineering Structures, 43, 21–30. http://doi.org/10.1016/j.engstruct.2012.05.003

Caracoglia, L., Jones, N. P., 2003. A methodology for the experimental extraction of indicial functions for streamlined and bluff deck sections. Journal of Wind Engineering and Industrial Aerodynamics, 91, 609–636. http://doi.org/10.1016/S0167-6105(02)00473-7

Chen, Z. Q., Yu, X. D., Yang, G., Spencer, B. F., 2005. Wind-Induced Self-Excited Loads on Bridges. Journal of Structural Engineering, 131, 1783–1793. http://doi.org/10.1061/(ASCE)0733-9445(2005)131:12(1783)

Chowdhury, A. G., Sarkar, P. P., 2003. A new technique for identification of eighteen flutter derivatives using a three-degree-of-freedom section model. Engineering Structures, 25, 1763–1772. http://doi.org/10.1016/j.engstruct.2003.07.002

Chowdhury, A. G., Sarkar, P. P., 2005. Experimental identification of rational function coefficients for time-domain flutter analysis. Engineering Structures, 27, 1349–1364. http://doi.org/10.1016/j.engstruct.2005.02.019

Cigada, A., Falco, M., Zasso, A., 2001. Development of new systems to measure the aerodynamic forces on section models in wind tunnel testing. Journal of Wind Engineering and Industrial Aerodynamics, 89, 725–746. http://doi.org/10.1016/S0167-6105(01)00075-7

Costa, C., 2007. Aerodynamic admittance functions and buffeting forces for bridges via indicial functions. Journal of Fluids and Structures, 23(3), 413–428. http://doi.org/10.1016/j.jfluidstructs.2006.10.002

Costa, C., Borri, C., 2006. Application of indicial functions in bridge deck aeroelasticity. Journal of Wind Engineering and Industrial Aerodynamics, 94(11), 859–881. http://doi.org/10.1016/j.jweia.2006.06.007

Diana, G., Fiammenghi, G., Belloli, M., Rocchi, D., 2013. Wind tunnel tests and numerical approach for long span bridges: The Messina bridge. Journal of Wind Engineering and Industrial Aerodynamics, 122, 38–49. http://doi.org/10.1016/j.jweia.2013.07.012

Diana, G., Resta, F., Zasso, a., Belloli, M., Rocchi, D., 2004. Forced motion and free motion aeroelastic tests on a new concept dynamometric section model of the Messina suspension bridge. Journal of Wind Engineering and Industrial Aerodynamics, 92, 441–462. http://doi.org/10.1016/j.jweia.2004.01.005

Diana, G., Rocchi, D., Argentini, T., Muggiasca, S., 2010. Aerodynamic instability of a bridge deck section model: Linear and nonlinear approach to force modeling. Journal of Wind Engineering and Industrial Aerodynamics, 98(6–7), 363–374. http://doi.org/10.1016/j.jweia.2010.01.003

Diana, G., Rocchi, D., Belloli, M., 2015. Wind tunnel : a fundamental tool for long-span bridge design. Structure and Infrastructure Engineering: Maintenance, Management, Life-Cycle Design and Performance, 11(4), 533–555. http://doi.org/10.1080/15732479.2014.951860

Falco, M., Curami, A., Zasso, A., 1992. Nonlinear effects in sectional model aeroelastic parameters identification. Journal of Wind Engineering and Industrial Aerodynamics, 42, 1321–1332. http://doi.org/10.1016/0167-6105(92)90140-6

Fenerci, A., Øiseth, O., 2015. Full-ScaleMeasurements on the Hardanger Bridge During StrongWinds. In Dynamics of Civil Structures, Volume 2, Conference Proceedings of the Society for Experimental Mechanics Series (Vol. 2, pp. 237–245). http://doi.org/10.1007/978-3-319-15209-7

Fung, Y., 1955. An introduction to the theory of aeroelasticity. Wiley.

Ge, Y. J., Xiang, H. F., 2008. Recent development of bridge aerodynamics in China. Journal of Wind Engineering and Industrial Aerodynamics, 96, 736–768. http://doi.org/10.1016/j.jweia.2007.06.045

Han, Y., Liu, S., Hu, J. X., Cai, C. S., Zhang, J., Chen, Z., 2014. Experimental study on aerodynamic derivatives

of a bridge cross-section under different traffic flows. Journal of Wind Engineering and Industrial Aerodynamics, 133, 250–262. http://doi.org/10.1016/j.jweia.2014.08.003

Huang, L., Liao, H., Wang, B., Li, Y., 2009. Numerical simulation for aerodynamic derivatives of bridge deck. Simulation Modelling Practice and Theory, 17(4), 719–729. http://doi.org/10.1016/j.simpat.2008.12.004

Jones, N. P., Scanlan, R. H., Sarkar, P. P., Singha, L., 1995. The effect of section model details on aeroelastic parameters. Journal of Wind Engineering and Industrial Aerodynamics, 54–55(C), 45–53. http://doi.org/10.1016/0167-6105(94)00028-C

Kareem, A., 2008. Numerical simulation of wind effects: A probabilistic perspective. Journal of Wind Engineering and Industrial Aerodynamics, 96(10–11), 1472–1497. http://doi.org/10.1016/j.jweia.2008.02.048

Kareem, A., Wu, T., 2014. Nonlinear Bluff-Body Aerodynamics. Analysis, Modeling and Applications. Lap Lambert Academic Publishing.

Körlin, R., Starossek, U., 2007. Wind tunnel test of an active mass damper for bridge decks. Journal of Wind Engineering and Industrial Aerodynamics, 95(4), 267–277. http://doi.org/10.1016/j.jweia.2006.06.015

Lee, S. H., Kwon, S.-D., 2009. A simple apparatus for measuring self-excited wind forces on bridges. In The Seventh Asia-Pacific Conference on Wind Engineering, Taipei.

Li, Q. C., 1995. Measuring flutter derivatives for bridge sectional models in water channel. Journal of Engineering Mechanics, 121(7093), 90–101.

Matsuda, K., Cooper, K. R., Tanaka, H., Tokushige, M., Iwasaki, T., 2001. An investigation of Reynolds number effects on the steady and unsteady aerodynamic forces on a 1:10 scale bridge deck section model. Journal of Wind Engineering and Industrial Aerodynamics, 89, 619–632. http://doi.org/10.1016/S0167-6105(01)00062-9

Matsumoto, M., 1996. Aerodynamic damping of prisms. Journal of Wind Engineering and Industrial Aerodynamics, 59, 159–175. http://doi.org/10.1016/0167-6105(96)00005-0

Matsumoto, M., Shiraishi, N., Shirato, H., Shigetaka, K., Niihara, Y., 1993. Aerodynamic derivatives of coupled/hybrid flutter of fundamental structural sections. Journal of Wind Engineering and Industrial Aerodynamics, 49(1), 575–584. http://doi.org/10.1016/0167-6105(93)90051-O

Neuhaus, C., Roesler, S., Höffer, R., Hortmanns, M., & Zahlten, W., 2009. Identification of 18 Flutter Derivatives by Forced Vibration Tests – A New Experimental Rig. In 5th European and African Conference on Wind Engineering, Florence.

Qin, X. R., Kwok, K. C. S., Fok, C. H., Hitchcock, P. A., 2009. Effects of frequency ratio on bridge aerodynamics determined by free-decay sectional model tests. Wind and Structures, 12(5), 413–424.

Salvatori, L., Borri, C., 2007. Frequency- and time-domain methods for the numerical modeling of full-bridge aeroelasticity. Computers and Structures, 85(11–14), 675–687. http://doi.org/10.1016/j.compstruc.2007.01.023

Sarkar, P. P., Caracoglia, L., & Haan, F. L. (2007). Parametric Study of Flutter Derivatives of Bridge Cross Sections and Their Implications on the Aeroelastic Stability of Flexible Bridges. In Proceedings of the 39th joint meeting of U.S.-Japan panel on wind and seismic effects UJNR, Tsukuba.

Sarkar, P. P., Caracoglia, L., Haan, F. L., Sato, H., Murakoshi, J., 2009. Comparative and sensitivity study of flutter derivatives of selected bridge deck sections, Part 1: Analysis of inter-laboratory experimental data. Engineering Structures, 31(1), 158–169. http://doi.org/10.1016/j.engstruct.2008.07.020

Sarkar, P. P., Chowdhury, a. G., Gardner, T. B., 2004. A novel elastic suspension system for wind tunnel section model studies. Journal of Wind Engineering and Industrial Aerodynamics, 92, 23–40. http://doi.org/10.1016/j.jweia.2003.09.036

Sarkar, P. P., Scanlan, R. H., Jones, N. P., 1994. Identification of aeroelastic parameters of flexible bridges. Journal of Engineering Mechanics, 120(8), 1718–1742.

Sarwar, M. W., Ishihara, T., Shimada, K., Yamasaki, Y., Ikeda, T., 2008. Prediction of aerodynamic characteristics of a box girder bridge section using the LES turbulence model. Journal of Wind Engineering and Industrial Aerodynamics, 96(10–11), 1895–1911. http://doi.org/10.1016/j.jweia.2008.02.015

Scanlan, R. H., 1978. The action of flexible bridges under wind. I flutter theory. Journal of Sound and Vibration, 60(2), 187–199.

Scanlan, R. H., 1997. Amplitude and Turbulence Effects on Bridge Flutter Derivatives. Journal of Structural Engineering, 123(2), 232–236. http://doi.org/10.1061/(ASCE)0733-9445(1997)123:2(232)

Scanlan, R. H., Jones, N. P., Lorendeaux, O., 1997. Comparison of taut-strip and section-model-based approaches in long-span bridge aerodynamics. Journal of Wind Engineering and Industrial Aerodynamics, 72, 275–287. http://doi.org/10.1016/S0167-6105(97)00250-X

Scanlan, R. H., Tomko, J., 1971. Airfoil and bride deck flutter derivaitves. Journal of Engineering Mechanics Div, 97(6), 1717–33.

Shinozuka, M., 1972. Monte Carlo solution of structural dynamics. Computers and Structures, 2(5–6), 855–874.

http://doi.org/10.1016/0045-7949(72)90043-0
Shinozuka, M., Jan, C.-M., 1972. Digital simulation of random processes and its applications. Journal of Sound and Vibration, 25(1), 111–128. http://doi.org/10.1016/0022-460X(72)90600-1
Siedziako, B., Øiseth, O., Rönnquist, A., 2016. Identification of Aerodynamic Properties of Bridge Decks in Arbitrary Motion. In Special Topics in Structural Dynamics, Volume 6: Proceedings of the 34th IMAC, A Conference and Exposition on Structural Dynamics (pp. 79–85). http://doi.org/10.1007/978-1-4614-6546-1
Svend Ole Hansen ApS., 2009. The Hardanger Bridge. Static and dynamic wind tunnel tests with a section model Prepared for: Norwegian Public Roads Administration Revision 2, March 2009.
Theodorsen, T., 1935. General theory of aerodynamic instability and the mechanism of flutter. NACA Report. http://doi.org/10.1017/CBO9781107415324.004
Ukeguchi, N., Sakata, H., Nishitani, H., 1966. An investigation of aerolastic initability of suspension bridges. In Symposium on Suspension Bridges, Lisbon.
Wardlaw, R. L., 1980. Sectional versus full model wind tunnel testing of bridge road decks. Proceedings of the Indian Academy of Sciences Section C: Engineering Sciences, 3, 177–198. http://doi.org/10.1007/BF02861559
West, G. S., Apelt, C. J., 1982. The effects of tunnel blockage and aspect ratio on the mean flow past a circular cylinder with Reynolds numbers between 10^4 and 10^5. Journal of Fluid Mechanics, 114, 361–377. http://doi.org/http://dx.doi.org/10.1017/S0022112082000202
Xu, F. Y., Wu, T., Ying, X. Y., Kareem, A., 2016. Higher-order Self-Excited Drag Forces on Bridge Decks. Journal of Engineering Mechanics, 142(3), 1–11. http://doi.org/10.1061/(ASCE)EM.1943-7889.0001036
Zasso, A., Belloli, M., Argentini, T., Flamand, O., Knapp, G., Grillaud, G., Klein, J-F, Virlogeux ., de Ville, V., 2014. Third Bosporus Bridge aerodynamics: Sectional and fulll-aerolastic model testing. In Istanbul Bridge Conference, Istanbul.
Zhang, Z., Chen, Z., Asce, M., Cai, Y., Ge, Y., 2011. Indicial Functions for Bridge Aeroelastic Forces and Time-Domain Flutter Analysis. Journal of Bridge Engineering, 16, 546–557. http://doi.org/10.1061/(ASCE)BE.1943-5592.0000176.
Zhang, Z. T., Chen, Z. Q., 2010. Indicial functions for bridge aero-elastic forces and discussion of some problematic issues in flutter analysis. In The Fifth International Symposium on Computational Wind Engineering (CWE2010). Chapel Hill.
Zhu, Z. W., Gu, M., Chen, Z. Q., 2007). Wind tunnel and CFD study on identification of flutter derivatives of a long-span self-anchored suspension bridge. Computer-Aided Civil and Infrastructure Engineering, 22(8), 541–554. http://doi.org/10.1111/j.1467-8667.2007.00509.x
Øiseth, O., Rönnquist, A., Kvåle, K. A., Sigbjörnsson, R., 2015. Monitoring Wind Velocities and Dynamic Response of the Hardanger Bridge. In Dynamics of Civil Structures, Volume 2, Conference Proceedings of the Society for Experimental Mechanics Series (Vol. 2, pp. 117–125). http://doi.org/10.1007/978-3-319-15248-6
Øiseth, O., Rönnquist, A., Sigbjörnsson, R., 2010. Simplified prediction of wind-induced response and stability limit of slender long-span suspension bridges, based on modified quasi-steady theory: A case study. Journal of Wind Engineering and Industrial Aerodynamics, 98(12), 730–741. http://doi.org/10.1016/j.jweia.2010.06.009
Øiseth, O., Rönnquist, A., Sigbjörnsson, R., 2011. Time domain modeling of self-excited aerodynamic forces for cable-supported bridges: A comparative study. Computers and Structures, 89(13–14), 1306–1322. http://doi.org/10.1016/j.compstruc.2011.03.017
Øiseth, O., Rönnquist, A., & Sigbjörnsson, R. (2012). Finite element formulation of the self-excited forces for time-domain assessment of wind-induced dynamic response and flutter stability limit of cable-supported bridges. Finite Elements in Analysis and Design, 50, 173–183. http://doi.org/10.1016/j.finel.2011.09.008